A&A, 684, L20 (2024)
https://doi.org/10.1051/0004-6361/202449716

Astronomy & Astrophysics

LETTER TO THE EDITOR

Age of (152830) Dinkinesh I Selam constrained by secular tidal-BYORP theory

C. C. Merrill[1], A. R. Kubas[1], A. J. Meyer[2], and S. D. Raducan[3]

[1] Cornell University, Ithaca, NY 14853, USA
e-mail: ccm242@cornell.edu
[2] University of Colorado, Boulder, CO 80303, USA
[3] University of Bern, Bern, Switzerland

Received 23 February 2024 / Accepted 5 April 2024

ABSTRACT

We constrained the age of the main belt binary asteroid system, (152830) Dinkinesh, through secular dynamics and assuming the secondary, Selam, is at equilibrium. We reproduced Selam's current semi-major axis and rotation period and Dinkinesh's current rotation period, starting from the initial conditions of the spin-up fission event. The method presented here includes the secular effects of YORP, BYORP, and tidal interactions, while also allowing for the strengths of these effects to be constrained. Based on this method, we performed a Monte Carlo simulation, which indicates that Selam's age is likely to be ∼1–10 Ma. Derivations for improved equations that describe tidal-BYORP equilibria in binary asteroid systems are also presented in this work. In particular, we derived: (1) a tidal-BYORP equilibrium equation that scales appropriately with the secondary mass and accounts for differences in the primary and secondary densities; and (2) an equation for YORP-driven primary spin stability, with the secondary being at equilibrium.

Key words. celestial mechanics – minor planets, asteroids: general – planets and satellites: dynamical evolution and stability

1. Introduction

Binary asteroid systems account for 15% of the near-Earth asteroid population between 200 m and 10 km in diameter (Pravec 2006; Margot et al. 2002). Nearly all asteroids in this size range are expected to be rubble piles (see review in Walsh 2018) and the dominant theory for binary system formation is the rotational fission of a rubble pile (Walsh et al. 2008; Rubincam 2000). This fission occurs when the Yarkovsky-O'Keefe-Radzievskii-Paddack (YORP) effect increases the spin rate of the parent body (or primary) until it reaches a critical spin rate where the centrifugal acceleration on the surface material supersedes the body's gravitational acceleration (Rubincam 2000; Vokrouhlický & Capek 2002). Material is then lofted from the surface and a satellite (or secondary) is formed by accretion beyond the Roche limit of the primary (Walsh et al. 2008, 2012). After forming, the secondary will synchronize with the primary due to tidal effects (typically on the order of 10^5 years, Goldreich & Sari 2009). The secondary's long-term orbital evolution will then be dominated by the binary-YORP (BYORP) effect and tides (Ćuk & Burns 2005). Both the BYORP effect and tides can either expand or contract the secondary's semi-major axis but tides tend to be expansive, as the spin rate of the primary is almost always greater than the orbit rate of the secondary (McMahon & Scheeres 2010b; Pravec 2006). This follows naturally from the rotational fission theory for binary systems: the primary's fast spin is typically preserved as the secondary forms; thus, many binary systems feature fast-rotating primaries (e.g., Didymos's period is 2.2600 ± 0.0001 h Scheirich & Pravec 2022). Tides and BYORP change the energy and angular momentum in the system and may cause the secondary to migrate and reach the Hill radius or impact the primary (Ćuk 2007; McMahon & Scheeres 2010a).

On November 1, 2023, NASA's Lucy spacecraft flew by the main belt asteroid, (152830) Dinkinesh, which it observed to be a binary system (Levison et al. 2024). The only other small binary asteroid system visited by a spacecraft is the near-Earth system, (65803) Didymos (Daly et al. 2023; Chabot et al. 2024). The Dinkinesh and Didymos systems share remarkable similarities, which help to highlight their differences and makes their comparison particularly enriching. Although the primary body (hereafter, Dinkinesh) has a similar size and spectral type to Didymos, it differs in terms of its morphological features, as Dinkinesh has large troughs and steep walls that appear to be absent on Didymos (Levison et al. 2024; Barnouin et al. 2024). The secondary of the Dinkinesh system, Selam, differs from Dimorphos in many aspects, including its size, shape, and mass (Chabot et al. 2024). In Table 1, we summarize the key comparisons between the Didymos and Dinkinesh systems. Selam is a definitively unique secondary and is the first contact binary observed as the secondary in a binary system (Levison et al. 2024). Contact binaries have been observed in the near-Earth population, the main belt, the Jupiter-family comets, and the Kuiper belt. They likely make up between 14% and 30% of small bodies larger than 200 meters (Virkki et al. 2022). Some of these bodies may have been formed via reaccumulation after disruption (presented as a mechanism to form Itokawa in Michel & Richardson 2013) while others may be primordial bodies (e.g., Arrokoth, McKinnon et al. 2020; Marohnic et al. 2021) or formed via low-speed collisions (Jutzi & Asphaug

Table 1. Characteristics of the Didymos and Dinkinesh binary systems with 1σ uncertanties.

Parameter	Didymos [(a)]	Dinkinesh [(b)]
Volume-equivalent diameter of primary [m]	730 ± 17	719 ± 24
Volume-equivalent diameter of secondary [m]	150.0 ± 2.5	282 ± 28
Bulk density of primary, secondary [kg m^{-3}]	2790 ± 140, 2400 ± 300	2400 ± 350
Semi-major axis [m]	1189 ± 17	3110 ± 50
Secondary shape	Oblate ellipsoid	Bilobate
Mutual orbital period [h]	11.921493 ± 0.000016	52.67 ± 0.04
Mutual orbital eccentricity	<0.03	0
Primary rotation period [h]	2.2600 ± 0.0001	3.7387 ± 0.0013
Heliocentric semi-major axis [AU]	1.64266506 [(c)]	2.1915426 [(c)]
Heliocentric eccentricity	0.383264789 [(c)]	0.1121065 [(c)]

Notes. The semi-major axis is the orbital semi-major axis rather than a semi-axis of an ellipsoid shape model. [(a)]Appendix of Chabot et al. (2024), [(b)]Levison et al. (2024), and [(c)]JPL (2024).

2015). The creation of contact binaries in binary systems has been discussed in the context of secondary fission as a possible mechanism (Jacobson & Scheeres 2011a). Because of the diversity of these objects and lack of formation observations, they have also been the subject of recent mission designs (e.g., Merrill et al. 2024). Despite the extensive literature that focuses on contact binaries, the bilobate shape of Selam remains a puzzle. In this paper, we aim to contribute to the solution of this puzzle by constraining the age of the system through dynamical simulations. The results from this study can be compared to ages derived by crater size-frequency analyses and, when combined with these analyses, could provide insight into the dynamical history of the system (e.g., Barnouin et al. 2024).

2. Methods

2.1. YORP theory

The YORP effect is a torque on asteroid bodies driven by solar radiation pressure. An extensive derivation of YORP torques is given in Scheeres (2007), but we only consider the leading-order form of this effect, outlined in Rossi et al. (2009). The rate of change of the spin rate of the primary from YORP is

$$\dot{\omega}_{\mathrm{p,Y}} = \frac{H_\odot}{2\pi R_\mathrm{p}^2 \rho_\mathrm{p}} C_\mathrm{Y}, \tag{1}$$

where R_p is the radius of a volume-equivalent sphere for the primary, ρ_p is the density of the primary, C_Y is the normalized YORP coefficient,

$$H_\odot = \frac{F_\odot}{a_\odot^2 \sqrt{1-e_\odot^2}}, \tag{2}$$

$F_\odot = 10^{17}$ N, $a_\odot$ is the heliocentric semi-major axis, and $e_\odot$ is the heliocentric eccentricity. Rossi et al. (2009) found that applying a Gaussian distribution of $C_\mathrm{Y} = 0 \pm 0.0125$ (1σ) successfully reproduced the spin rates of bodies in the near-Earth population.

2.2. BYORP theory

We refer to McMahon & Scheeres (2010a,b) and Cueva et al. (2024) for extensive BYORP theory development and applications, as we only offer a summary of the effect here. We use a leading-order BYORP theory based on the year-averaged equations from McMahon & Scheeres (2010a). The rate of change to the semi-major axis due to the BYORP effect is

$$\dot{a}_\mathrm{B} = \frac{3H_\odot}{2\pi\rho_\mathrm{s} R_\mathrm{s}} \sqrt{\frac{a^3(1-e^2)}{\mu}} B, \tag{3}$$

where $\mu = G(M_\mathrm{p} + M_\mathrm{s})$ is the standard gravitational parameter of the system, G is the gravitational constant, M_p is the mass of the primary, M_s is the mass of the secondary, a is the semi-major axis of the secondary, e is the eccentricity of the secondary, R_s is the radius of a volume-equivalent sphere for the secondary, ρ_s is the density of the secondary, and B is the normalized BYORP coefficient given by

$$B = \frac{\mathbf{A}_0(2)}{R_\mathrm{s}^2}. \tag{4}$$

Here, $\mathbf{A}_0(2)$ is the along-track component of the zeroth-order Fourier coefficient in the secondary's body-fixed frame presented in McMahon & Scheeres (2010a,b) and Scheeres (2007). In particular, B is a difficult parameter to predict for asteroids and has a strong dependence on the body's shape and surface topography. A nearly-synchronous secondary is necessary for the BYORP effect (Ćuk & Burns 2005). Non-synchronous motion will effectively "turn off" this effect, as there will no longer be a consistent portion of the body interacting with the solar radiation pressure and the torques exerted on the body will net 0 (Quillen et al. 2022). It appears that Selam is tidally locked and so, we can assume that BYORP is active (Levison et al. 2024).

2.3. Tidal theory

To account for tidal effects, we use the classical tidal theory presented in Chapt. 4.9 of Murray & Dermott (1999). The magnitude of the tidal torque of the secondary on the primary is given by

$$\Gamma = \frac{3}{2}\frac{k}{Q}\frac{G M_\mathrm{s}^2 R_\mathrm{p}^5}{a^6}, \tag{5}$$

where k is the primary's tidal Love number and Q is the primary's tidal quality factor. The tidal torque can be related to the rate of change in mechanical energy with

$$\dot{E} = \begin{cases} -\Gamma(\omega_\mathrm{p} - n) & \text{when } \omega_\mathrm{p} > n \\ 0 & \text{when } \omega_\mathrm{p} = n \\ \Gamma(\omega_\mathrm{p} - n) & \text{when } \omega_\mathrm{p} < n \end{cases} \tag{6}$$

where n is the mean motion of the secondary. This can be related to the rate of change in the semi-major axis due to tides with

$$\dot{E} = -\frac{1}{2}\frac{M_p M_s}{M_p + M_s} n a \dot{a}_T (\omega_p - n). \tag{7}$$

Rearranging the equation for $\dot{a}_T$ and substituting in Eq. (6) results in

$$\dot{a}_T = sign(\omega_p - n) 3n \frac{k}{Q} \frac{M_s}{M_p} \frac{R_p^5}{a^4} \tag{8}$$

which is the change in semi-major axis due to tidal torque. The tidal torque's effect on the primary's spin is given by

$$\dot{\omega}_{p,T} = -sign(\omega_p - n) \frac{3k}{2\alpha Q} \frac{G M_s^2 R_p^3}{M_p a^6}, \tag{9}$$

from Murray & Dermott (1999), where we assume $\alpha = 2/5$. In this work, we adopted the convention derived in Nimmo & Matsuyama (2019), where tidal dissipation is primarily driven by the surface layer of regolith on the asteroid. Pou & Nimmo (2024) combined this work with that of Goldreich & Sari (2009), which solves for k/Q via Eqs. (16) and (12) in Pou & Nimmo (2024) to obtain

$$\frac{k}{Q} = 9.81 \times 10^{-22} \frac{t^2 \rho_p^2 M_p}{n^2 R_p M_s} \tag{10}$$

where t is the regolith thickness and the leading constant has units of $m^5\ kg^{-2}\ s^{-2}$. The constant is computed with a yield strain of $\epsilon_Y = 10^{-2}$ and rigidity $\mu^* = 10^{10}$ Pa for individual boulders, which are the values used in Nimmo & Matsuyama (2019) and Pou & Nimmo (2024). These values were selected because they are typical for rubble pile bodies and this allows us to maintain consistency between this study and Nimmo & Matsuyama (2019) and Pou & Nimmo (2024). This approach is adopted solely to constrain k/Q bounds and discussed to explain where uncertainty in k/Q can arise; we highlight that it is not meant to constrain the surface properties of Dinkinesh.

2.4. Tidal-BYORP equilibrium

There is an equilibrium semi-major axis where expansive tides and contractive BYORP (i.e., $B < 0$) are equal and opposite (i.e., $\dot{a}_B + \dot{a}_T = 0$, Jacobson & Scheeres 2011b). In typical binary systems, where the primary's spin rate is greater than the secondary's mean motion (i.e., $\omega_p > n$), this equilibrium semi-major axis, a_{eq}, is stable. For such systems, when $a < a_{eq}$, tidal effects are stronger than BYORP and increase the semi-major axis back to a_{eq}. When $a > a_{eq}$, BYORP effects are stronger than tidal effects and shrink the semi-major axis to a_{eq} and so the equilibrium is stable. This ratio of B, Q, and k can then be found as

$$\frac{|B|Q}{k} = \frac{2\pi \rho_s^2 \mu R_p^2 R_s^4}{\rho_p H_\odot a_{eq}^7}, \tag{11}$$

where a_{eq} is the equilibrium semimajor axis that the secondary will asymptotically converge to for $B < 0$ and $\omega_p > n$. We solve for a_{eq} to obtain

$$a_{eq} = \left(\frac{k}{|B|Q} \frac{2\pi \rho_s^2 \mu R_p^2 R_s^4}{\rho_p H_\odot} \right)^{1/7}. \tag{12}$$

These equations are qualitatively similar to those in Jacobson & Scheeres (2011b) but are more accurate for more massive secondaries, as they scale with the mass of the secondary and account for differences in the primary and secondary densities. It appears that Eq. (3) in Jacobson & Scheeres (2011b) mistakenly uses the reduced mass of the system rather than the secondary mass, which leads to an error in computation. Assuming the secondary and primary densities are equal and the secondary is of negligible mass, Eq. (11) will be equal to Eq. (11) from Jacobson & Scheeres (2011b). However, we recommend the use of this work's equations in future studies to ensure accuracy.

2.5. Primary spin stability

The tidal-BYORP equilibrium we discuss here is a stable equilibrium, with the assumption that the primary's spin does not evolve substantially. If the primary's spin is reduced such that $\omega_p = n$, a doubly-synchronous system is achieved which may destabilize small secondaries (Jacobson et al. 2014). If the primary's spin is increased, it may further undergo fission, which could also destabilize the system. Thus, the tidal-BYORP equilibrium, alone, is not necessarily a final state for binary systems due to the primary's changing spin state. However, if the spin of the primary is kept constant, then the system can theoretically exist in the stable equilibrium for perpetuity. This stable equilibrium requires that the torque on the primary from tides is equivalent to the torque provided by the YORP effect (i.e., $\dot{\omega}_{p,Y} + \dot{\omega}_{p,T} = 0$, Golubov et al. 2018). We set Eq. (1) equal to Eq. (9) to solve for the semi-major axis:

$$a_Y = \left| \frac{k}{C_Y Q} \frac{4\pi^2 G R_p^2 R_s^6 \rho_p^2}{H_\odot \alpha} \right|^{1/6} \tag{13}$$

where the torque on the primary from YORP and tides are equal and opposite. When $a > a_Y$, the torque from YORP will dominate the spin evolution of the primary and when $a < a_Y$, the torque from tides will dominate the spin evolution of the primary. There is a special case where $a_Y = a_{eq}$ and this is when:

$$C_Y = -B \frac{2\pi \rho_p^3 a_{eq} G R_s^2}{\rho_s^2 \mu \alpha}. \tag{14}$$

Here, the primary's spin will not evolve when the secondary's semi-major axis is a_{eq}. We note that C_Y is actually a function of the primary and Eq. (14) should only be used to estimate C_Y if a system is found to be particularly long-lived and stable. The stability for this condition is as follows: if BYORP is contractive and tides are expansive (i.e., $\omega_p > n$ and $B < 0$), then a secondary at a_{eq} will be stable (Jacobson & Scheeres 2011b). If C_Y is equivalent to Eq. (14) and tidal torques are negative (i.e., $C_Y > 0$ and $\omega_p > n$), then the primary spin will also be stabilized (Golubov et al. 2018). If any of these three conditions are not fulfilled ($\omega_p > n$, $B < 0$, and $C_Y > 0$), the secondary's orbit and primary's spin will not be stabilized simultaneously. It is possible that the system will leave this state when either body experiences a significant impact or the system has a close encounter with a planet. However, there appears to be no effect internal to the system that could destabilize it.

2.6. Monte Carlo analysis

We produce a Monte Carlo analysis to obtain statistical data on the age of Selam. Here, the "age" is the time starting from the

Table 2. Variables and distributions used for the Monte Carlo analysis.

Parameter	Variable type	Mean value $\pm 1\sigma$; [bounds]	Note and source
Final mutual orbit period [h]	Fixed	52.67	Mottola et al. (2023)
Eccentricity	Fixed	0	Levison et al. (2024)
Diameter of Dinkinesh [m]	Gaussian	719 ± 24	Levison et al. (2024)
Diameter of Selam [m]	Gaussian	282 ± 28	Levison et al. (2024)
a_{eq} [m]	Gaussian	3110 ± 50	Levison et al. (2024)
k/Q	Log-Uniform	10^{-x}; $x \in (3, 5)$	x is uniformly distributed
Coefficient for YORP	Gaussian	0 ± 0.0125 ; [−2, Eq. (14)]	Rossi et al. (2009)
Coefficient for BYORP	Derived	Eq. (11)	Contractive BYORP only
Density [kg m^{-3}]	Derived	$3\pi a_{eq}^3/(P^2 G(R_p^3 + R_s^3))$	–
Initial primary spin [rad s^{-1}]	Derived	Eq. (15)	Angular momentum conservation
Initial semi-major axis [m]	Uniform	$(1.5R_p, 2.5R_p)$	Roche limit

Notes. The diameters of Dinkinesh and Selam are volume-equivalent sphere diameters. In the density equation, P is the mutual orbital period.

formation of Selam to the current system's state. Table 2 lists the variables used in the tests and describes how they are varied. It is assumed in these tests that the current semi-major axis of Selam is equivalent to a_{eq}, which is a reasonable assumption given that Selam appears to be in synchronous rotation and has no measurable eccentricity (Levison et al. 2024). The coefficient of YORP, C_Y, has a well-defined normal distribution (Rossi et al. 2009) but we only accept values of C_Y that are less than the value in Eq. (14). Because the spin of the primary is initially faster than the current spin rate, we require the primary to slow down (i.e., C_Y must not be greater than the value given by Eq. (14) or else the primary will tend to speed up in time and never reach its current spin rate). To constrain the k/Q values, we use Eq. (10), with a regolith thickness of $10\,\mathrm{m} < t < 100\,\mathrm{m}$, which results in $10^{-5} < k/Q < 10^{-3}$; these are typical k/Q values for rubble piles (Nimmo & Matsuyama 2019; Pou & Nimmo 2024). With the assumption that the system is at a_{eq}, this results in $10^{-4} < |B| < 10^{-2}$, which is also a typical range for B magnitudes (Jacobson & Scheeres 2011b). We only considered contractive BYORP, as this is a necessary condition for our a_{eq} assumption to hold.

We uniformly distributed Selam's initial semimajor axis between the Roche limits for bodies with strength and zero cohesion ($1.5R_p < a_i < 2.5R_p$, Holsapple & Michel 2006, 2008). Dinkinesh's initial spin rate derived via angular momentum conservation is

$$\omega_p = \frac{\alpha(M_p + M_s)(R_p^3 + R_s^3)^{2/3}\omega_d - M^* \sqrt{\mu a_i} - \alpha M_s R_s^2 n}{\alpha M_p R_p^2}, \quad (15)$$

where $\omega_d = \sqrt{4\pi G\rho_p/3}$ is the disruption spin rate of a sphere and $M^* = M_p M_s/(M_p + M_s)$ is the reduced mass of the system (Pravec et al. 2010). We note that we effectively treat Selam as a single body that formed immediately after the disruption of Dinkinesh. Despite the morphological complexity of Selam, this is a reasonable assumption given that Agrusa et al. (2024) found that ∼8% of fission events create more than a single secondary within the first 100 days and an early impact is much more likely than a persisting multi-body system Ferrari et al. (2024). We assume the synchronization timescale is small compared to the timescale for orbit evolution. This is a fitting assumption given that the synchronization timescale should be no greater than $\sim 10^5$ years (Goldreich & Sari 2009; Levison et al. 2024); however, could be as low as ∼1 year, as some secondaries form with nearly synchronous spin (Agrusa et al. 2024). The maximum age we allowed our simulations to produce is 1 Ga (i.e., the collisional lifetime of Dinkinesh-sized bodies, Richardson et al. 2022; Bottke et al. 2005; Raducan et al. 2024). The simulations were concluded when two conditions are simultaneously satisfied: (1) the period of the primary reaches 3.7387 hours and (2) the semi-major axis of the secondary is within 0.1% of a_{eq} (and, thus, the secondary has reached its equilibrium position). If either of these two criteria are not satisfied, the run is not counted, as it has not accurately modeled the Dinkinesh system's current state. We ran the simulation until we produced 10^6 cases that satisfy the two previously mentioned conditions. To offer some model validation, our model outputs are $\rho = 2420 \pm 260$ kg m^{-3} and $\mu = 33.1 \pm 1.6$ m^3/s^2, which are comparable to the current estimates for Dinkinesh ($\rho = 2400 \pm 350$ kg m^{-3}; $\mu = 33.0 \pm 1.6$ m^3/s^2; Levison et al. 2024).

3. Results and discussion

3.1. Selam's age

Although Selam's age spans four orders of magnitude in our Monte Carlo simulations, we find that ∼2/3 of runs conclude between 1–10 Ma. Figure 1 plots the resulting age and first, second, and third quartiles of 1.38, 2.97, and 7.18 Ma, respectively. The mode of the data (for 100 bins per order of magnitude) falls at 2.00–2.04 Ma. Ages of $>10^8$ years (∼1% of cases) indicate that C_Y is close to the equilibrium C_Y from Eq. (14) and are slow-evolving systems. We compare the age of Selam to that of Dimorphos (<0.3 Ma; Barnouin et al. 2024), reasoning that Selam is likely to be an older secondary than Dimorphos would be. The short lifetimes of these objects indicate that binary systems are continuously created.

Selam's rate of orbit expansion is sensitive to the magnitudes of k/Q and B. For a given k/Q, the time it takes Selam to reach its current semi-major axis is the minimum age in Fig. 2. This minimum age can be reduced if Selam formed further from the Roche limit or if Selam is not at a_{eq}. As previously mentioned, the age of Selam should be independently derived via crater analysis. Given that age, constraints may be placed on k/Q and C_Y (e.g., if Selam's age is the mode of our data, 2 Ma, then $C_Y > -1.0\text{e}{-2}$ and $k/Q > 6.0\text{e}{-5}$ from Fig. 2). We note that Selam being at equilibrium does not exclude periods of non-synchronous rotation (e.g., tumbling or barrel instability), but those periods should be short compared to Selam's age (Ćuk et al. 2021; Meyer et al. 2023b). In short-timescale simulations, the irregular shapes of Dinkinesh and Selam are important to model because of their spin-orbit coupling (e.g., Meyer et al.

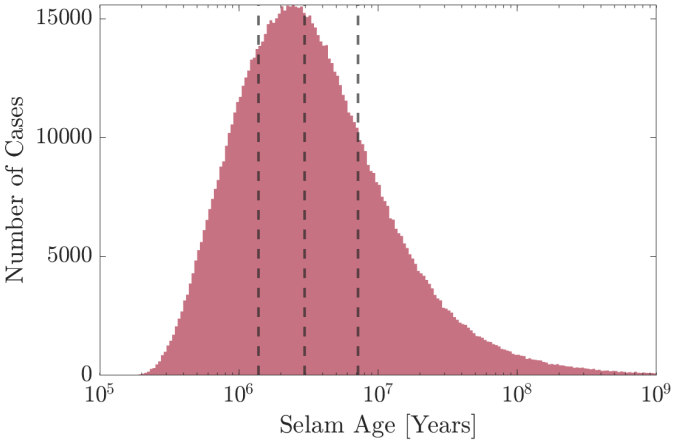

Fig. 1. Age of Selam from the Monte Carlo simulation (1 million cases). The vertical dashed gray lines are placed at the first, second, and third quartiles of 1.38, 2.97, and 7.18 Ma, respectively. The bins are logarithmically spaced such that there are 50 bins for each order of magnitude.

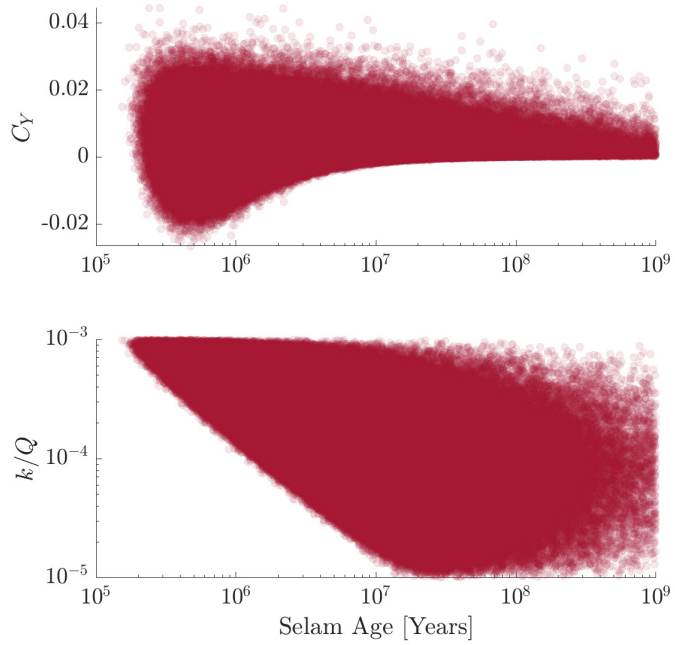

Fig. 2. Effects of YORP and tides on Selam's age (1 million cases).

2023a), but these short-period processes should not alter our results.

3.2. BQ/k for Dinkinesh and Didymos

Assuming Selam's current semimajor axis is a_{eq}, Dinkinesh's BQ/k magnitude is 10.1 ± 3.8, which is more than an order of magnitude lower than BQ/k for pre-DART Didymos (358 ± 108 found using the data in Richardson et al. 2024). A potential explanation for Dinkinesh's lower BQ/k magnitude is Selam's bilobate shape, which could cause significant self-shadowing and weaken the BYORP effect. If self-shadowing is indeed the primary reason for the lower BQ/k value, this will have implications for other bilobate bodies and contact binaries in general. Because of the constraint placed on k/Q and the derived BQ/k relation, we may also constrain $|B|$ (e.g., $k/Q > 6e{-}5$ indicates $|B| > 6.1e{-}4 \pm 2.3e{-}4$).

4. Conclusions

We derived an improved version of the tidal-BYORP equilibrium equation that scales appropriately with the mass of the secondary and accounts for the difference in density between the primary and secondary. We defined the necessary conditions for a coefficient of YORP that will stabilize the spin of the primary when the secondary is at a_{eq}. A system in this state has a stronger stability condition than one strictly characterized by BYORP and tides. Ultimately, we find that only external factors could destabilize such a system.

We reproduced the orbital state of Dinkinesh and Selam starting from spin-fission conditions using tidal, BYORP, and YORP effects. We find that the Dinkinesh system has a much lower BQ/k magnitude than the Didymos system, which may be the result of self-shadowing but this requires further investigation. Our Monte Carlo simulation indicates that Selam has an age of 1–10 Ma, with a median age of 3 Ma and it is likely to be older than Dimorphos. If Selam's absolute age is measured by crater analysis with a higher level of accuracy than that achieved this work, further constraints may be placed on C_Y, k/Q, B, and the system's dynamical history.

Acknowledgements. We thank both Rachel Cueva and our reviewer, Seth Jacobson, whom improved the quality of this paper. We also thank Phil Nicholson, Dmitry Savransky, Charlie Detelich, Veronica Hegelein, and the H.M. folks for their discussions and support.

References

Agrusa, H. F., Zhang, Y., Richardson, D. C., et al. 2024, Planet. Sci. J., 5, 54
Barnouin, O., Ballouz, R.-L., Marchi, S., et al. 2024, Nat. Commun., submitted
Bottke, W. F., Durda, D. D., Nesvorný, D., et al. 2005, Icarus, 179, 63
Chabot, N. L., Rivkin, A. S., Cheng, A. F., et al. 2024, Planet. Sci. J., 5, 49
Cueva, R. H., McMahon, J. W., Meyer, A. J., et al. 2024, Planet. Sci. J., 5, 48
Ćuk, M. 2007, ApJ, 659, L57
Ćuk, M., & Burns, J. A. 2005, Icarus, 176, 418
Ćuk, M., Jacobson, S. A., & Walsh, K. J. 2021, Planet. Sci. J., 2, 231
Daly, R. T., Ernst, C. M., Barnouin, O. S., et al. 2023, Nature, 616, 443
Ferrari, F., Panicucci, P., Merisio, G., et al. 2024, Nat. Commun., submitted
Goldreich, P., & Sari, R. 2009, ApJ, 691, 54
Golubov, O., Unukovych, V., & Scheeres, D. J. 2018, ApJ, 857, L5
Holsapple, K. A., & Michel, P. 2006, Icarus, 183, 331
Holsapple, K. A., & Michel, P. 2008, Icarus, 193, 283
Jacobson, S. A., & Scheeres, D. J. 2011a, Icarus, 214, 161
Jacobson, S. A., & Scheeres, D. J. 2011b, ApJ, 736, L19
Jacobson, S. A., Scheeres, D. J., & McMahon, J. 2014, ApJ, 780
JPL 2024, Small-Body Database Lookup, https://ssd.jpl.nasa.gov/tools/sbdb_lookup.html#/
Jutzi, M., & Asphaug, E. 2015, Nature, 348, 1355
Levison, H. F., Marchi, S., Noll, K. S., et al. 2024, Nature, submitted
Margot, J. L., Nolan, M. C., Benner, L. A. M., et al. 2002, Science, 296, 1445
Marohnic, J., Richardson, D., McKinnon, W., et al. 2021, Icarus, 356, 113824
McKinnon, W. B., Richardson, D. C., Marohnic, J. C., et al. 2020, Science, 367, eaay6620
McMahon, J., & Scheeres, D. 2010a, Icarus, 209, 494
McMahon, J., & Scheeres, D. 2010b, Celest. Mech. Dyn. Astron., 106, 261
Merrill, C. C., Geiger, C. J., Tahsin, A. T. M., Savransky, D., & Peck, M. 2024, Acta Astron., 214, 629
Meyer, A. J., Agrusa, H. F., Richardson, D. C., et al. 2023a, Planet. Sci. J., 4, 141
Meyer, A. J., Scheeres, D. J., Agrusa, H. F., et al. 2023b, Icarus, 391, 115323
Michel, P., & Richardson, D. C. 2013, A&A, 554
Mottola, S., Denk, T., Marchi, S., et al. 2023, MNRAS, 524, L1
Murray, C. D., & Dermott, S. F. 1999, Solar System Dynamics (Cambridge University Press)
Nimmo, F., & Matsuyama, I. 2019, Icarus, 321, 715
Pou, L., & Nimmo, F. 2024, Icarus, 411, 115919
Pravec, P., et al. 2006, Icarus, 181, 63

Pravec, P., Vokrouhlický, D., Polishook, D., et al. 2010, Nat. Lett., 466, 1085
Quillen, A. C., LaBarca, A., & Chen, Y. 2022, Icarus, 374, 114826
Raducan, S. D., Jutzi, M., Merrill, C. C., et al. 2024, Planet. Sci. J., 5, 79
Richardson, D. C., Agrusa, H. F., Barbee, B., et al. 2022, Planet. Sci. J., 3, 157
Richardson, D. C., Agrusa, H. F., Barbee, B., et al. 2024, Planet. Sci. J., submitted
Rossi, A., Marzari, F., & Scheeres, D. 2009, Icarus, 202, 95
Rubincam, D. P. 2000, Icarus, 148, 2
Scheeres, D. 2007, Icarus, 188, 430
Scheirich, P., & Pravec, P. 2022, Planet. Sci. J., 3, 163
Virkki, A. K., Marshall, S. E., Venditti, F. C. F., et al. 2022, Planet. Sci. J., 3, 222
Vokrouhlický, D., & Capek, D. 2002, Icarus, 159, 449
Walsh, K. J. 2018, ARA&A, 56, 593
Walsh, K. J., Richardson, D. C., & Michel, P. 2008, Nature, 454, 188
Walsh, K. J., Richardson, D. C., & Michel, P. 2012, Icarus, 220, 514